

Optimal reconstruction of the Hellings and Downs correlation

Bruce Allen*

Max Planck Institute for Gravitational Physics (Albert Einstein Institute),
Leibniz Universität Hannover, Callinstraße 38, D-30167, Hannover, Germany

Joseph D. Romano†

Department of Physics and Astronomy, University of Texas Rio Grande Valley,
One West University Boulevard, Brownsville, TX 78520, USA

(Dated: August 26, 2024)

Pulsar timing arrays (PTAs) detect gravitational waves (GWs) via the correlations they create in the arrival times of pulses from different pulsars. The mean correlation, a function of the angle between the directions to two pulsars, was predicted in 1983 by Hellings and Downs (HD). Observation of this angular pattern is the “smoking gun” that GWs are present, so PTAs “reconstruct the HD curve” by estimating the correlation using pulsar pairs separated by similar angles. Several studies have examined the amount by which this curve is expected to differ from the HD mean. The variance arises because (a) a finite set of pulsars at specific sky locations is used, (b) the GW sources interfere, and (c) the data are contaminated by noise. Here, for a Gaussian ensemble of sources, we predict that variance by constructing an optimal estimator of the HD correlation, taking into account the pulsar sky locations and the frequency distribution of the GWs and the pulsar noise. The variance is a ratio: the numerator depends upon the pulsar sky locations, and the denominator is the (effective) number of frequency bins for which the GW signal dominates the noise. In effect, after suitable combination, each frequency bin gives an independent estimate of the HD correlation.

Introduction.—As pulsar timing arrays (PTAs) work towards 5σ detections of gravitational waves (GWs) [1–4], there is growing interest in different aspects of the underlying physics. This includes potential GW sources, mechanisms that influence pulsar rotation, and the propagation, detection, and analysis of electromagnetic pulses. These, in turn, inform the data analysis.

If GWs had large amplitudes, their effects on the arrival times of pulses from a single pulsar would be directly visible. Early work [5] set upper limits on the GW amplitude using individual pulsars, but it is now known that GW effects are small compared to pulsar timing noise. So, to detect GWs, PTAs search for GW-induced correlations in the arrival times of pulses from *different* pulsars.

The correlation $-1 \leq \frac{3}{2}\mu \leq 1$ in pulsar timing residuals is a function of the angle $\gamma \in [0, \pi]$ between the directions to pulsars. These “spatial” or “angular” correlations can be expressed as a sum of Legendre polynomials

$$\mu(\gamma) = \sum_l c_l P_l(\cos \gamma). \quad (1)$$

The coefficients c_l are estimated from the data: 100 pulsars would give values of μ at 4950 angles $\gamma > 0$.

The expected pattern of correlation for a stationary, isotropic and unpolarized gravitational wave background (GWB) was predicted in 1983 by Hellings and Downs (HD). This function μ_u is plotted in the top panel of Fig. 1 and is called the “HD curve” [6]:

$$\begin{aligned} \mu_u(\gamma) &\equiv \langle \mu(\gamma) \rangle = \sum_l \langle c_l \rangle P_l(\cos \gamma) \\ &= \frac{1}{3} + \frac{1 - \cos \gamma}{2} \left[\ln \left(\frac{1 - \cos \gamma}{2} \right) - \frac{1}{6} \right]. \end{aligned} \quad (2)$$

The expected coefficients $\langle c_0 \rangle = 0$, $\langle c_1 \rangle = 0$, and

$$\langle c_l \rangle = (2l + 1)/((l + 2)(l + 1)l(l - 1)) \text{ for } l \geq 2, \quad (3)$$

are computed in [7–9]. (The correlation is doubled to $3\mu_u(0) = 1$ for pulsars that are closer together than the typical GW wavelength [10, App. C.2].) Detection of the HD curve provides evidence that the pulsar arrival time fluctuations are due to GWs [11].

How closely will the correlations in our (realization of the) Universe follow this curve? Even if the noise is small, deviations occur because of (1) pulsar variance and (2) cosmic variance. The first arises because observations are carried out with a finite set of pulsars at specific sky locations [12]. The second arises because our Universe has a discrete set of GW sources with specific frequencies, sky locations, and other parameters. Interference between these GW sources means that even if (1) is eliminated by using many pulsars [10, 13, 14], the pulsar-averaged correlation curve [15] will still differ from the HD curve.

We quantify such deviations via the variance

$$\sigma_\mu^2(\gamma) \equiv \langle \mu(\gamma)^2 \rangle - \langle \mu(\gamma) \rangle^2, \quad (4)$$

noting that its value and meaning depend upon the statistical ensemble used for the angle brackets.

Previous work.—The question was first addressed by Roebber and Holder [8]. They assumed that the GWB is described by an isotropic and unpolarized Gaussian ensemble of sources radiating GWs at a single frequency, and that noise-free measurements are carried out using an infinite number of pulsars. While not given in this

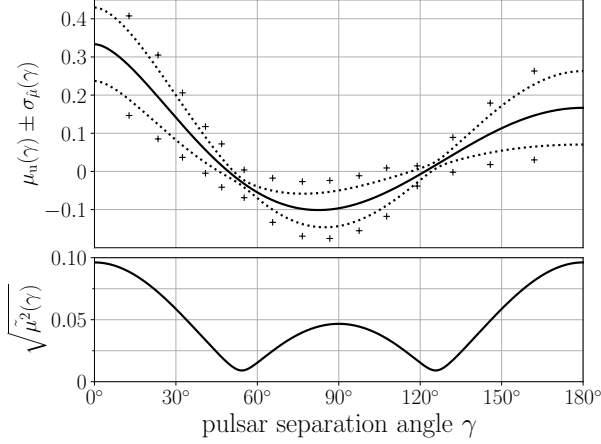


FIG. 1. Top: the black line is the HD curve $\mu_u(\gamma)$ of (2). The “+” symbols are the predicted $\sigma_u = \pm 1\sigma_G$ deviations of (34), for a reconstruction using NANOGrav’s [2] 15 angular bins and 67 pulsars, if $N_f = 1$. The dotted line is the same prediction in the limit of an infinite number of pulsars (8). Bottom: square root of the function $\tilde{\mu}^2(\gamma)$ of (5).

form (see [10, App. C6] and [16]), they obtain

$$\sigma_\mu^2(\gamma) = \tilde{\mu}^2(\gamma) \equiv \sum_l \frac{\langle c_l \rangle^2}{2l+1} P_l^2(\cos \gamma), \quad (5)$$

whose square root is shown in the bottom panel of Fig. 1. This follows from a sky-map decomposition of the GWB into spherical harmonics $Y_{lm}(\Omega_p)$ where Ω_p is the pulsar location on the two-sphere [9]. For fixed l , there are $(2l+1) \times 2$ (GW polarizations) real amplitudes. Each is an independent Gaussian random variable, so the c_l are χ^2 distributed with $k = 4l+2$ degrees of freedom. Since this distribution has mean k and variance $2k$, the ratio of the variance to the squared mean is $2/k = 1/(2l+1)$ as seen in (5). This variance was also found in [10] [with a closed form for $\tilde{\mu}^2(\gamma)$, Eq. (G11)], where it was shown to arise from interference between GW sources.

More recent work examines the effects of pulsar variance and cosmic variance [10]. Using the “pulsar averaging” technique of Cornish and Sesana [15], this shows how to separate pulsar and cosmic variance. These are computed for a Gaussian ensemble with an arbitrary spectrum, and for two different discrete-source ensembles, each containing N circularly polarized GW sources. If the GW sources radiate at different frequencies and do not interfere, then the cosmic variance vanishes. In contrast, if the sources radiate at the same frequency, then interference produces cosmic variance. In the limit $N \rightarrow \infty$, this recovers the Roebber and Holder result, provided that the density of sources approaches infinity with the strength of each source vanishing in a way that keeps the mean-squared strain at Earth constant. These results have also been extended to ensembles of N elliptically polarized GW sources, corresponding to circular binaries with randomly oriented orbital planes [17].

These studies compute the cosmic variance for a large number of pulsars, uniformly spread on the sky. Later work shows how to combine measurements from a finite set of pulsars at specific sky locations, to produce a minimum variance estimator of the HD correlation [12]. It proves that the cosmic variance of the Gaussian ensemble is the variance of the optimal estimator of the pulsar-averaged correlation, in the limit of large numbers of uniformly distributed pulsars, and shows how the transition from pulsar variance to cosmic variance takes place, as more pulsars are added to a PTA [12, e.g., Fig. 7].

In all of this previous work, the quantity used to estimate the correlation μ was a general linear combination of the “zero-lag” time-averaged product of redshifts

$$\rho_{ab} \equiv \overline{Z_a(t)Z_b(t)} \equiv \frac{1}{T} \int_{-T/2}^{T/2} dt Z_a(t)Z_b(t). \quad (6)$$

Here, a, b label pulsars, $Z_a(t)$ is the redshift of pulsar a at time t on Earth, and overbar denotes the average over observation time T . The linear combination of ρ_{ab} was picked to form an unbiased, minimum variance estimator.

Summary.—In this paper, we construct the best possible estimator $\hat{\mu}$ of the HD correlation for a Gaussian ensemble using a finite set of pulsar pairs in an angular bin at angle γ . The estimator (26) combines the data in frequency, also incorporating nonzero-lag information. Our main result: the variance of the estimator is

$$\sigma_{\hat{\mu}}^2 = \frac{\sigma_G^2}{N_f}. \quad (7)$$

Here, σ_G^2 is a geometric quantity, determined entirely by the pulsar-pair locations, and $N_f \geq 0$ is the (effective, noninteger) number of frequency bins for which the GWB dominates the pulsar noise. If the angular bin is narrow, and contains many pulsar pairs uniformly distributed on the sky, then $\sigma_G^2 \rightarrow \tilde{\mu}^2(\gamma)$ and (7) becomes

$$\sigma_{\hat{\mu}}^2 = \frac{1}{N_f} \tilde{\mu}^2(\gamma) \iff \sigma_{c_l}^2 = \frac{1}{N_f} \frac{\langle c_l \rangle^2}{2l+1}. \quad (8)$$

This generalizes the Roebber and Holder [8] $N_f = 1$ result (5). Figure 2 illustrates how the variance $\sigma_{\hat{\mu}}^2$ of the optimal estimator and the number of signal-dominated frequency bins N_f vary as a function of the squared SNR ρ^2 (44), for a simple numerical example.

Derivation.—In the Earth-pulsar neighborhood, far from any GW sources, GWs are described by a plane-wave expansion [10, Eq. (C1)]. The transverse traceless synchronous metric perturbations arising from GWs are

$$h_{\mu\nu}(t, \mathbf{x}) = \sum_A \int df \int d\Omega h_A(f, \Omega) e_{\mu\nu}^A(\Omega) e^{2\pi i f(t - \Omega \cdot \mathbf{x})}, \quad (9)$$

where the spatial coordinate $\mathbf{x} = 0$ at Earth and time t is measured there. In (9), the GW frequency $f \in \mathfrak{R}$,

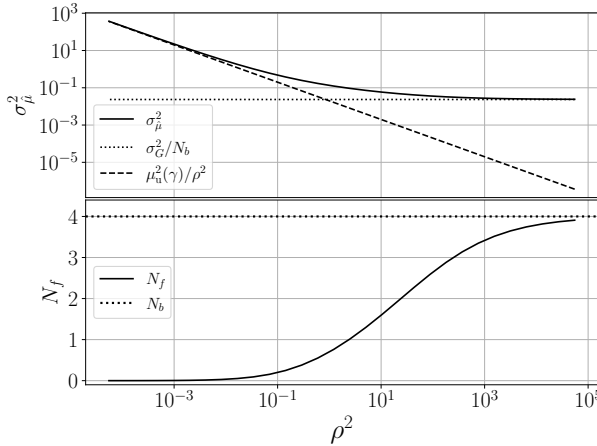


FIG. 2. Variance $\sigma_{\hat{\mu}}^2$ of the reconstructed HD curve (top) and number of signal-dominated frequency bins N_f (bottom) as a function of squared SNR ρ^2 . For small SNR, N_f is small, and $\sigma_{\hat{\mu}}^2$ is pulsar-noise dominated. For large SNR, N_f approaches $N_b = 4$, and $\sigma_{\hat{\mu}}^2$ is cosmic-variance dominated.

and the unit vector $\boldsymbol{\Omega}$ is the GW propagation direction, touching the unit two-sphere at spherical polar coordinates $\Omega = (\theta, \phi)$. The infinitesimal area on the sphere is $d\Omega = \sin \theta d\theta d\phi$, the spatial coordinate indices $\mu, \nu \in x, y, z$, the polarization label $A \in +, \times$, the polarization tensors $e_{\mu\nu}^+$ and $e_{\mu\nu}^\times$ depend upon the GW direction, and h_+ and h_\times are arbitrary complex functions satisfying $h_A^*(f, \Omega) = h_A(-f, \Omega)$, since $h_{\mu\nu}$ is real.

Consider a pulsar a at distance $L_a > 0$ from Earth in direction $\boldsymbol{\Omega}_a$, so $\mathbf{x}_a = L_a \boldsymbol{\Omega}_a$. The redshift of the pulsar's frequency at time t on Earth

$$Z_a(t) = z_a(t) + n_a(t) \quad (10)$$

is the sum of a GW-induced term $z_a(t)$ and a pulsar noise term $n_a(t)$, given by Fourier transforms

$$\begin{aligned} z_a(t) &= \sum_A \int df \int d\Omega h_A(f, \Omega) F_a^A(\Omega) \tau(f, L_a \boldsymbol{\Omega}_a, \Omega) e^{2\pi i f t} \\ n_a(t) &= \int df \tilde{n}_a(f) e^{2\pi i f t}. \end{aligned} \quad (11)$$

The pulsar “antenna pattern” for polarization A is

$$F_a^A(\Omega) = \frac{1}{2} \frac{\Omega_a^\mu \Omega_a^\nu e_{\mu\nu}^A(\Omega)}{1 + \boldsymbol{\Omega} \cdot \boldsymbol{\Omega}_a}, \quad (12)$$

with the Einstein summation convention applying to μ and ν . The factor τ forms the difference between Earth and pulsar terms [13]:

$$\tau(f, L_a \boldsymbol{\Omega}_a, \Omega) = 1 - e^{-2\pi i f L_a (1 + \boldsymbol{\Omega} \cdot \boldsymbol{\Omega}_a)}. \quad (13)$$

Expressions (9), (10), and (11) describe the GWs and the redshift over intervals (millions of years) much shorter than the Hubble time; PTAs observe a snapshot of the redshift (10) over a time interval T of order decades.

Assume that the redshift is observed over a time period $t \in [-T/2, T/2]$. Standard observational practice represents this as a Fourier sum

$$Z_a(t) = \sum_j Z_a^j e^{2\pi i f_j t} \text{ for } t \in [-T/2, T/2], \quad (14)$$

where the frequencies $f_j \equiv j/T$ are integer multiples of $1/T$. The sum has $j \in -N_b, \dots, -1, 1, \dots, N_b$, where N_b is the number of frequency bins. For quantities that carry both pulsar and frequency indices, we put pulsar indices a, b, c, d, e, f down and frequency indices j, k, ℓ, m up.

Multiplying the expressions in (11) by $T^{-1} e^{-2\pi i f_k t}$ and integrating over $t \in [-T/2, T/2]$, and then doing the same to (14) gives the redshift amplitude in the k 'th frequency bin, $Z_a^k \equiv z_a^k + n_a^k$, with

$$\begin{aligned} n_a^k &= \int df \tilde{n}_a(f) \text{sinc}(\pi(f - f_k)T) \\ z_a^k &= \sum_A \int df \int d\Omega h_A(f, \Omega) F_a^A(\Omega) \times \\ &\quad \tau(f, L_a \boldsymbol{\Omega}_a, \Omega) \text{sinc}(\pi(f - f_k)T). \end{aligned} \quad (15)$$

The $\text{sinc } x \equiv (\sin x)/x$ sidelobes arise from sources whose frequencies are not integer multiples of $1/T$. Since (11) are real, $z_a^{k*} = z_a^{-k}$, $n_a^{k*} = n_a^{-k}$, and $Z_a^{k*} = Z_a^{-k}$.

Since the pulsar noises $n_a(t)$ are unknown, and the parameters (sky positions, frequencies, amplitudes, etc.) of the GW sources contributing to $h_A(f, \Omega)$ are unknown, we cannot predict the redshifts. Instead, we give a statistical description, assuming that the GWs and pulsar noise arise independently from incoherent sums of many weak sources. The central limit theorem applies, so both are described by stationary Gaussian processes.

Let $h_A(f, \Omega)$ and $\tilde{n}_a(f)$ be representative functions drawn from stationary Gaussian ensembles describing an isotropic unpolarized GWB and uncorrelated pulsar noise. Then, using angle brackets to denote averages over this ensemble, the Gaussian process is fully defined by its first $\langle h_A(f, \Omega) \rangle = \langle \tilde{n}_a(f) \rangle = 0$ and second moments

$$\begin{aligned} \langle h_A(f, \Omega) h_{A'}^*(f', \Omega') \rangle &= \delta_{AA'} \delta(f - f') \delta^2(\Omega, \Omega') H(f), \\ \langle \tilde{n}_a(f) \tilde{n}_b^*(f') \rangle &= \delta_{ab} \delta(f - f') N_a(f), \\ \langle \tilde{h}_A(f, \Omega) \tilde{n}_b^*(f') \rangle &= 0, \end{aligned} \quad (16)$$

where $H(f) = H(-f) \geq 0$ and $N_a(f) = N_a(-f) \geq 0$ are real power spectra of the GWB and noise ([10, Eqns.(C5-7)] relates $H(f)$ to the GW energy density and other observables). The δ_{ab} term in (16) reflects our assumption that the noise in the different pulsars is statistically independent. All higher moments can be computed from the first and second moments via Isserlis's theorem [18].

The Fourier coefficients Z_a^k are linear combinations of $h_A(f, \Omega)$ and $\tilde{n}_a(f)$, so they are also Gaussian random variables. Their first moments $\langle Z_a^k \rangle = 0$, and from (15) and (16) their second moments are

$$\langle Z_a^j Z_b^{k*} \rangle = H_{jk} \mu_{ab} + N_a^{jk} \delta_{ab}. \quad (17)$$

Here, $\mathbf{H} \equiv H_{jk}$ and $\mathbf{N}_a = N_a^{jk}$ are real bisymmetric $2N_b \times 2N_b$ matrices

$$\begin{aligned} H_{jk} &\equiv 4\pi \int df H(f) \operatorname{sinc}(\pi(f-f_j)T) \operatorname{sinc}(\pi(f-f_k)T) , \\ N_a^{jk} &\equiv 4\pi \int df N_a(f) \operatorname{sinc}(\pi(f-f_j)T) \operatorname{sinc}(\pi(f-f_k)T) \end{aligned} \quad (18)$$

with rows/columns indexed by frequency bin. They have nonnegative eigenvalues, and their matrix inverses are denoted for example by \mathbf{H}^{-1} ; if $\det(\mathbf{H}) = 0$, then \mathbf{H}^{-1} denotes the Moore-Penrose pseudoinverse. Since $H_{jk} = H_{kj} = H_{-k,-j}$, both \mathbf{H} and \mathbf{H}^{-1} are reflection invariant across either diagonal; the same holds for \mathbf{N}_a .

The object $\mu \equiv \mu_{ab}$ that appears in (17) is

$$\mu \equiv \mu_{ab} \equiv \mu_u(\gamma_{ab})(1 + \delta_{ab}) . \quad (19)$$

It has indices labeled by pulsars a and b , and its entries are the values of the HD curve at angle γ_{ab} , doubled if a and b are the same. The angle $\gamma_{ab} \in [0, \pi]$ between the lines of sight to a and b is defined by $\cos \gamma_{ab} = \mathbf{\Omega}_a \cdot \mathbf{\Omega}_b$.

To obtain (17) and (19), we used the definition of the Hellings and Downs curve

$$\mu_u(\gamma_{ab}) \equiv \frac{1}{4\pi} \sum_A \int d\Omega F_a^A(\Omega) F_b^A(\Omega) , \quad (20)$$

and the reasoning given in [10, App. C2] to replace

$$\tau(f, L_a \mathbf{\Omega}_a, \mathbf{\Omega}) \tau^*(f, L_b \mathbf{\Omega}_b, \mathbf{\Omega}) \rightarrow 1 + \delta_{ab} \quad (21)$$

within integrals over frequency f and direction Ω .

Later, we need the covariance

$$\begin{aligned} C_{ab,cd}^{jk,\ell m} &\equiv \langle Z_a^j Z_b^k Z_c^{\ell*} Z_d^{m*} \rangle - \langle Z_a^j Z_b^k \rangle \langle Z_c^{\ell*} Z_d^{m*} \rangle \\ &= \langle Z_a^j Z_c^{\ell*} \rangle \langle Z_b^k Z_d^{m*} \rangle + \langle Z_a^j Z_d^{m*} \rangle \langle Z_b^k Z_c^{\ell*} \rangle \\ &= \mu_{ac} \mu_{bd} H_{j\ell} H_{km} + \mu_{ad} \mu_{bc} H_{jm} H_{k\ell} + \\ &\quad \delta_{ac} \mu_{bd} N_a^{j\ell} H_{km} + \delta_{ad} \mu_{bc} N_a^{jm} H_{k\ell} + \\ &\quad \mu_{ac} \delta_{bd} H_{j\ell} N_b^{km} + \mu_{ad} \delta_{bc} H_{jm} N_b^{k\ell} + \\ &\quad \delta_{ac} \delta_{bd} N_a^{j\ell} N_b^{km} + \delta_{ad} \delta_{bc} N_a^{jm} N_b^{k\ell} , \end{aligned} \quad (22)$$

where the second equality follows from Isserlis's theorem [18], and the third from (17). For reasons described below, we need the part of $C_{ab,cd}^{jk,\ell m}$ which is symmetric in both jk and ℓm :

$$\mathbf{C} \equiv C_{ab,cd}^{jk,\ell m} \equiv C_{ab,cd}^{(jk),(\ell m)} , \quad (23)$$

where the round brackets denote symmetrization, e.g., $Q_{(jk)} \equiv (Q_{jk} + Q_{kj})/2$. It is easy to see that the noise-free component of $C_{ab,cd}^{jk,\ell m}$ factors into

$$C_{ab,cd}^{jk,\ell m} |_{\mathbf{N}=0} = G_{ab,cd} H_{j(\ell} H_{m)k} . \quad (24)$$

The “geometry” part depends on the pulsar directions:

$$\mathbf{G} \equiv G_{ab,cd} \equiv \mu_{ac} \mu_{bd} + \mu_{ad} \mu_{bc} , \quad (25)$$

and plays an important role in [12].

To estimate the HD correlation at angle γ , we use N_{pair} pulsar pairs ab lying in an angular bin around γ . Following [12], we use the notation $ab \in \gamma$ to denote this set of pulsar pairs; autocorrelations are excluded, so $a < b$. See [12, Fig. 2] for a helpful illustration with $N_{\text{pair}} = 3$.

The estimator $\hat{\mu}$ is a general linear combination

$$\hat{\mu} \equiv \sum_{ab \in \gamma} \sum_{jk} W_{ab}^{jk} Z_a^j Z_b^k \quad (26)$$

of redshift cross-products. The weights $\mathbf{W} \equiv W_{ab}^{jk}$ are set by requiring that $\hat{\mu}$ (i) is unbiased, (ii) minimizes the variance among universes drawn from the Gaussian ensemble, and (iii) is real, so $W_{ab}^{jk*} = W_{ab}^{-j,-k}$. As discussed, this is more general than the estimator of [12], which is a linear combination of the zero-lag correlations (6)

$$\rho_{ab} \equiv \overline{Z_a(t) Z_b(t)} = \sum_j Z_a^j Z_b^{j*} , \quad (27)$$

where the final equality follows from substituting (14) into (6). Those estimators have frequency-independent weights W_{ab}^{jk} , which vanish off the antidiagonal $j = -k$. The more general form (26) allows us to further reduce the variance, thus improving the estimator.

The optimal weights W_{ab}^{jk} are found as in [12, Sec. 3A]. From (17), the ensemble average of the estimator (26) is

$$\langle \hat{\mu} \rangle = \sum_{ab \in \gamma} \sum_{jk} W_{ab}^{jk} \mu_{ab} \bar{H}_{jk} = \mu_u(\gamma) , \quad (28)$$

where the noise terms \mathbf{N} are absent because $a < b$. This is normalized to $\mu_u(\gamma)$ to ensure that $\hat{\mu}$ is unbiased. We have defined $\bar{H} \equiv \bar{H}_{jk} \equiv H_{j,-k}$; it is symmetric in jk since $H_{j,-k} = H_{-j,k} = H_{k,-j}$. Since (28) does not constrain the part of W_{ab}^{jk} antisymmetric in jk , we set that to zero: $W_{ab}^{jk} = W_{ab}^{kj} = W_{ab}^{(jk)}$.

The variance (4) of the estimator $\hat{\mu}$ is

$$\begin{aligned} \sigma_{\hat{\mu}}^2 &\equiv \langle |\hat{\mu}|^2 \rangle - |\langle \hat{\mu} \rangle|^2 \\ &= \sum_{ab \in \gamma} \sum_{cd \in \gamma} \sum_{jk} \sum_{\ell m} W_{ab}^{jk} C_{ab,cd}^{jk,\ell m} W_{cd}^{\ell m*} . \end{aligned} \quad (29)$$

The second equality follows from (22), (23), and (26). The rhs of (29) motivates the introduction of an inner product between weights $\mathbf{A} \equiv A_{ab}^{jk}$ and $\mathbf{B} \equiv B_{cd}^{\ell m}$:

$$(\mathbf{A}, \mathbf{B}) \equiv \sum_{ab \in \gamma} \sum_{cd \in \gamma} \sum_{jk} \sum_{\ell m} A_{ab}^{jk} C_{ab,cd}^{jk,\ell m} B_{cd}^{\ell m*} . \quad (30)$$

This inner product is positive definite if the pulsar positions are generic, \mathbf{H} and \mathbf{N}_a have nonzero eigenvalues, and \mathbf{A} and \mathbf{B} are symmetric in the frequency indices.

The covariance \mathbf{C} is a rank $N_b(2N_b + 1)N_{\text{pair}}$ square symmetric matrix with $4N_b^2 N_{\text{pair}}$ rows/columns. It has $N_b(2N_b - 1)N_{\text{pair}}$ eigenvectors antisymmetric in jk with

eigenvalue zero. Its rank $N_b(2N_b + 1)N_{\text{pair}}$ Moore-Penrose pseudoinverse $\mathbf{C}^{-1} \equiv (C^{-1})_{ab,cd}^{jk,\ell m}$ satisfies

$$\begin{aligned} \sum_{cd \in \gamma} \sum_{\ell m} (C^{-1})_{ab,cd}^{jk,\ell m} C_{cd,ef}^{\ell m,rs} &= 2\delta_{a(e\delta_f)b}\delta_{r(j\delta_k)s} \\ &= \delta_{ae}\delta_{bf}\delta_{r(j\delta_k)s}, \end{aligned} \quad (31)$$

where the last equality holds if $a < b$ and $e < f$.

It is helpful to introduce real weights $\mathbf{V} \equiv \mathbf{C}^{-1} \boldsymbol{\mu} \bar{\mathbf{H}}$

$$\mathbf{V} \equiv V_{ab}^{jk} \equiv \sum_{cd \in \gamma} \sum_{\ell m} (C^{-1})_{ab,cd}^{jk,\ell m} \mu_{cd} \bar{H}_{\ell m}. \quad (32)$$

These are symmetric in jk and satisfy $V_{ab}^{jk*} = V_{ab}^{-j,-k}$.

To find the weights \mathbf{W} defining the minimum-variance estimator $\hat{\mu}$, use the inner product (30) to write

$$\langle \hat{\mu} \rangle = (\mathbf{W}, \mathbf{V}) \quad \text{and} \quad \sigma_{\hat{\mu}}^2 = (\mathbf{W}, \mathbf{W}). \quad (33)$$

The first equality follows from (28), (30), and (32), and the second from (29) and (30). Minimizing the variance subject to the normalization constraint $\langle \hat{\mu} \rangle = \mu_u(\gamma)$ is equivalent to minimizing the ratio $(\mathbf{W}, \mathbf{W})/(\mathbf{W}, \mathbf{V})^2$ by maximizing the denominator. Since (30) is positive definite, this implies that \mathbf{W} is proportional to \mathbf{V} . The correctly normalized solution is $\mathbf{W} = \mu_u(\gamma) \mathbf{V}/(\mathbf{V}, \mathbf{V})$.

The variance of the optimal estimator follows from (30), (31), (32) and (33), and is

$$\sigma_{\hat{\mu}}^2 = (\mathbf{W}, \mathbf{W}) = \frac{\mu_u^2(\gamma)}{(\mathbf{V}, \mathbf{V})} = \frac{\sigma_G^2}{N_f}. \quad (34)$$

Here, we have defined

$$\sigma_G^2 \equiv \frac{\mu_u^2(\gamma)}{2 \boldsymbol{\mu}^t \mathbf{G}^{-1} \boldsymbol{\mu}}, \quad (35)$$

$$N_f \equiv \frac{(\boldsymbol{\mu} \bar{\mathbf{H}})^t \mathbf{C}^{-1} (\boldsymbol{\mu} \bar{\mathbf{H}})}{2 \boldsymbol{\mu}^t \mathbf{G}^{-1} \boldsymbol{\mu}}. \quad (36)$$

The $N_{\text{pair}} \times N_{\text{pair}}$ square symmetric matrix \mathbf{G}^{-1} satisfies

$$\sum_{cd \in \gamma} G_{ab,cd}^{-1} G_{cd,ef} \equiv \delta_{ae}\delta_{bf} + \delta_{af}\delta_{be} = \delta_{ae}\delta_{bf}, \quad (37)$$

where the last equality holds for $a < b$ and $e < f$.

In (35) and (36), $\boldsymbol{\mu}$ and $\boldsymbol{\mu} \bar{\mathbf{H}}$ are column vectors with respective dimensions N_{pair} and $4N_b^2 N_{\text{pair}}$. The quantity σ_G^2 (shown in Fig. 1 for NANOGrav's [2] 67 pulsars and 15 angular bins) is the one-frequency-bin cosmic variance found in [12] for a specific finite set of pulsar pairs. Below, we show that N_f is the effective number of frequency bins for which the GW signal dominates the noise.

Equation (34) is our main result. It is similar to the variance found in [12], but smaller for the reasons given after (27). Furthermore, as an optimal estimator, it is independent of the form of the data (e.g., timing residuals versus redshifts), because the powers of f relating them cancel out of the products of \mathbf{H} , \mathbf{N}_a , \mathbf{H}^{-1} , and \mathbf{N}_a^{-1} .

If the angular bin is narrow, then $\boldsymbol{\mu} \approx \mu_u(\gamma) \mathbf{1}$, where $\mathbf{1} = (1, \dots, 1)^t$ is a column vector containing N_{pair} ones. For this narrow angular bin, discrete pulsar pair case

$$\sigma_G^2 = \frac{1}{2 \mathbf{1}^t \mathbf{G}^{-1} \mathbf{1}}. \quad (38)$$

If there are many pulsar pairs in a bin at angle γ , uniformly distributed on the sky, then [12] shows that $(\mathbf{1}^t \mathbf{G}^{-1} \mathbf{1})^{-1} \rightarrow 2\bar{\mu}^2(\gamma)$. For this case,

$$\sigma_G^2 \rightarrow \bar{\mu}^2(\gamma), \quad (39)$$

from which our other key result (8) follows from (34).

To see why N_f is the effective number of frequency bins for which the GWB dominates pulsar noise, consider the following simple model: (a) The pulsar noise spectrum is pulsar independent, so $N_a^{jk} = N_{jk}$. (b) Below some crossover frequency bin N_c there is only a GW signal. (c) Above frequency bin N_c there is only pulsar noise.

$$\begin{aligned} (b) &\implies N_{jk} = 0 \text{ if } |j| \leq N_c \text{ and/or } |k| \leq N_c. \\ (c) &\implies H_{jk} = 0 \text{ if } |j| > N_c \text{ and/or } |k| > N_c. \end{aligned} \quad (40)$$

With these assumptions, the matrix $H_{jk} + N_{jk}$ is block diagonal. Since the “signal part” and the “noise part” act on orthogonal subspaces, \mathbf{C}^{-1} is given by

$$(C^{-1})_{ab,cd}^{jk,\ell m} = G_{ab,cd}^{-1} H_{\ell(j) m}^{-1} H_{k m}^{-1} + 2\delta_{c(a\delta_b)d} N_{\ell(j) m}^{-1} N_{k m}^{-1}, \quad (41)$$

where \mathbf{H}^{-1} and \mathbf{N}^{-1} denote Moore-Penrose pseudoinverses, with respective ranks $2N_c$ and $2N_b - 2N_c$. Eq. (41) can be verified by inserting it and the symmetric part of (22) into (31), since (40) implies that any contraction of \mathbf{H} with \mathbf{N} vanishes. From (41) it follows that

$$(\boldsymbol{\mu} \bar{\mathbf{H}})^t \mathbf{C}^{-1} (\boldsymbol{\mu} \bar{\mathbf{H}}) = \boldsymbol{\mu}^t \mathbf{G}^{-1} \boldsymbol{\mu} \text{Tr}(\bar{\mathbf{H}} \mathbf{H}^{-1} \bar{\mathbf{H}} \mathbf{H}^{-1}), \quad (42)$$

so (36) implies that

$$\begin{aligned} N_f &= \frac{1}{2} \sum_{j,k,\ell,m} \bar{H}_{jk} \bar{H}_{\ell m} H_{j\ell}^{-1} H_{km}^{-1} \\ &= \frac{1}{2} \sum_{j,k,\ell,m} H_{j,-k} H_{\ell,-m} H_{j\ell}^{-1} H_{km}^{-1} = N_c, \end{aligned} \quad (43)$$

which is half the rank of \mathbf{H} or of \mathbf{H}^{-1} . (The final equality follows by relabeling $k \rightarrow -k$ and $m \rightarrow -m$, then using $H_{km}^{-1} = H_{-k,-m}^{-1}$.)

We can see that N_f vanishes for small signal-to-noise (SNR) S , where S is the optimal cross-correlation *detection statistic* for the pulsar pairs in the angular bin. S is defined by the rhs of (26), but with different weights \mathbf{w} . The weights are set to maximize the ratio of $\langle S \rangle^2$ in the *presence* of a GWB to $\langle S^2 \rangle$ in its *absence*; the ratio ρ^2 is the square of the expected SNR. Via the same reasoning leading to (34), one obtains

$$\rho^2 = \frac{(\mathbf{w}, \mathbf{C}_0^{-1} \bar{\mathbf{H}} \boldsymbol{\mu})_0^2}{(\mathbf{w}, \mathbf{w})_0} = (\boldsymbol{\mu} \bar{\mathbf{H}})^t \mathbf{C}_0^{-1} (\boldsymbol{\mu} \bar{\mathbf{H}}), \quad (44)$$

where the optimal weights are $\mathbf{w} = \mathbf{C}_0^{-1} \bar{\mathbf{H}} \boldsymbol{\mu}$. The subscripts 0 indicates that $\mathbf{H} = 0$ in the covariance matrix (22) and for \mathbf{C} inside the inner product (30).

If the pulsar noise \mathbf{N} is large then $\mathbf{C} \rightarrow \mathbf{C}_0$ and ρ^2 is small. It follows from (36) that $N_f \approx \rho^2 \sigma_G^2 / \mu_u^2(\gamma)$ is small and that $\sigma_u^2 = \sigma_G^2 / N_f \approx \mu_u^2(\gamma) / \rho^2$ is large. For this case, the variance of the optimal estimator of the HD correlation is large, and dominated by pulsar noise rather than by cosmic variance. [Note: for pulsar-independent noise, \mathbf{C}_0^{-1} is given by the second term on the rhs of (41), so (44) gives an expected squared SNR $\rho^2 = N_{\text{pair}} \text{Tr}(\mathbf{H} \mathbf{N}^{-1} \mathbf{H} \mathbf{N}^{-1})$.]

Conclusion.— Roebber and Holder [8, end of Sec. 4] write that “separate frequency bins can be considered as independent realizations of the same map”. The word “considered” is needed: since \mathbf{H} is nondiagonal, the maps are correlated and not independent. This is generic to PTAs, whose observational timespans are much shorter than the coherence time of their GW sources.

Our calculation proves that this intuition is correct. It gives a rigorous definition of the number of signal-dominated frequency bins N_f , showing that each provides an independent estimator of the HD correlation. Optimally combining the data reduces the total variance in proportion to N_f .

It is satisfying that these results also hold for finite numbers of pulsars at specific sky locations, not just in the infinite-pulsar limit, and apply to both timing residuals and redshifts. They hold equally for the variances of $\mu(\gamma)$ or for their harmonic coefficients c_l in (1).

Bayesian reconstruction of the HD correlation, starting from PTA data, produces posterior probability distributions for $\mu(\gamma)$ and c_l . Because it makes optimal use of all information, with reasonable priors, we expect the corresponding variances to be in good agreement with our frequentist predictions. This has already been successfully tested [see Eq. (24)][19] and can be used to characterize and validate simulations such as [20].

* bruce.allen@aei.mpg.de

† joseph.romano@utrgv.edu

- [1] J. Antoniadis *et al.* (EPTA and InPTA Collaborations), The second data release from the European Pulsar Timing Array: III. Search for gravitational wave signals, *Astronomy & Astrophysics* **678**, A50 (2023).
- [2] G. Agazie *et al.* (NANOGrav Collaboration), The NANOGrav 15 yr Data Set: Evidence for a Gravitational-wave Background, *The Astrophysical Journal Letters* **951**, L8 (2023).
- [3] D. J. Reardon *et al.* (PPTA Collaboration), Search for an Isotropic Gravitational-wave Background with the Parkes Pulsar Timing Array, *The Astrophysical Journal Letters* **951**, L6 (2023).

- [4] H. Xu *et al.* (CPTA Collaboration), Searching for the Nano-Hertz Stochastic Gravitational Wave Background with the Chinese Pulsar Timing Array Data Release I, *Research in Astronomy and Astrophysics* **23**, 075024 (2023).
- [5] V. M. Kaspi, J. H. Taylor, and M. F. Ryba, High-Precision Timing of Millisecond Pulsars. III. Long-Term Monitoring of PSRs B1855+09 and B1937+21, *Astrophys. J.* **428**, 713 (1994).
- [6] R. W. Hellings and G. S. Downs, Upper limits on the isotropic gravitational radiation background from pulsar timing analysis, *Astrophys. J.* **265**, L39 (1983).
- [7] J. Gair, J. D. Romano, S. Taylor, and C. M. F. Mingarelli, Mapping gravitational-wave backgrounds using methods from CMB analysis: Application to pulsar timing arrays, *Phys. Rev. D* **90**, 082001 (2014).
- [8] E. Roebber and G. Holder, Harmonic space analysis of pulsar timing array redshift maps, *Astrophys. J.* **835**, 21 (2017).
- [9] B. Allen, Pulsar timing array harmonic analysis and source angular correlations, arXiv:2404.05677 (2024), to appear in PRD, arXiv:2404.05677 [gr-qc].
- [10] B. Allen, Variance of the Hellings-Downs correlation, *PRD* **107**, 043018 (2023).
- [11] B. Allen, S. Dhurandhar, Y. Gupta, M. McLaughlin, P. Natarajan, R. M. Shannon, E. Thrane, and A. Vecchio, The International Pulsar Timing Array checklist for the detection of nanoHertz gravitational waves (2023), arXiv:2304.04767 [astro-ph.IM].
- [12] B. Allen and J. D. Romano, Hellings and Downs correlation of an arbitrary set of pulsars, *Phys. Rev. D* **108**, 043026 (2023).
- [13] J. D. Romano and B. Allen, Answers to frequently asked questions about the pulsar timing array Hellings and Downs curve, *Classical Quantum Gravity* **41**, 175008 (2024).
- [14] B. Allen, Will pulsar timing arrays observe the Hellings and Downs correlation curve?, in *18th Vulcano Workshop: Frontier Objects in Astrophysics and Particle Physics*, Vol. 74, edited by A. Antonelli, R. Fusco Femiano, A. Morselli, and G. C. Trinchero (2022) pp. 65–80.
- [15] N. J. Cornish and A. Sesana, Pulsar timing array analysis for black hole backgrounds, *Classical and Quantum Gravity* **30**, 224005 (2013).
- [16] R. C. Bernardo and K.-W. Ng, Pulsar and cosmic variances of pulsar timing-array correlation measurements of the stochastic gravitational wave background, *J. C. A. P.* **2022**, 046 (2022).
- [17] B. Allen and S. Valtolina, Pulsar timing array source ensembles, *Phys. Rev. D* **109**, 083038 (2024).
- [18] L. Isserlis, On a formula for the product-moment coefficient of any order of a normal frequency distribution in any number of variables, *Biometrika* **12**, 134 (1918), often called “Wick’s Theorem” by physicists, although Wick’s work was three decades later.
- [19] Y.-M. Wu, Y.-C. Bi, and Q.-G. Huang, The spatial correlations between pulsars for interfering sources in pulsar timing array and evidence for gravitational-wave background in NANOGrav 15-year data set (2024), arXiv:2407.07319 [astro-ph.CO].
- [20] B. Bécsy, N. J. Cornish, and L. Z. Kelley, Exploring realistic nanoHertz gravitational-wave backgrounds, *The Astrophysical Journal* **941**, 119 (2022).